Tetrahedron 67 (2011) 1628–1632

Contents lists available at ScienceDirect

Tetrahedron

journal homepage: www.elsevier.com/locate/tet

Functionalization of 'kite' shaped styryl end-capped benzodithiophene with ketone groups: synthesis, characterization and properties

Yahia Didane [a], Atsufumi Kumagai [b], Noriyuki Yoshimoto [b], Christine Videlot-Ackermann [a,*], Hugues Brisset [c,*]

[a] Centre Interdisciplinaire de Nanoscience de Marseille (CINaM), CNRS UPR 3118, Campus Luminy, Aix Marseille Université, Case 913, 13288 Marseille Cedex 09, France
[b] Graduate School of Engineering, Iwate University, 4-3-5 Ueda, Morioka 020-8551, Japan
[c] Laboratoire Matériaux Polymères-Interfaces-Environnement Marin (MAPIEM—EA 4323), Université du Sud Toulon-Var, ISITV, BP 56, 83162 La Valette du Var, France

ARTICLE INFO

Article history:
Received 1 December 2010
Received in revised form 4 January 2011
Accepted 5 January 2011
Available online 12 January 2011

Keywords:
Thiophene
Transistors
Semiconductor

ABSTRACT

We report the synthesis of a new bridged end-capped distyryldithiophene with ketone groups on the bridge: *E,E*-2,7′-bis((2-phenyl)-ethenyl)-benzo[2,1-*b*:3,4-*b*′]dithiophene-4,5-dione **1**. Optical and electrochemical properties of **1** in solution were investigated by UV–vis absorption and cyclic voltammetry and compared to the unsubstituted parent molecule (**KDS2T**). Morphology of **1**-based thin films was investigated by scanning electron microscopy (SEM) and the crystalline structure characterization by X-ray diffraction (XRD). Thin films were implemented as active layers into organic thin-film transistors (OTFT) in top contact configuration to evaluate the charge transport properties.

© 2011 Elsevier Ltd. All rights reserved.

1. Introduction

Molecular modification of oligothiophene is a topic of intensive investigations for the development of active components in organic field effect transistors (OFETs).[1–3] We have shown the exceptional stability of p-channel OFETs based on distyryloligothiophenes[4,5] recently confirmed by Fréchet et al.[6] and Ong et al.[7] Based on these considerations we have developed synthetic strategies to modify the structure of the distyryldithiophene (**DS2T**) to increase: (i) its electroaffinity to turn this compound into an n-type semiconductor,[8,9] (ii) the solubility for investigation of solution-processed organic thin-film transistors or sensors,[10–12] (iii) its charge carrier mobility by bridging the bithiophene core.[13] In the latter case, the bridged distyryldithiophene (**KDS2T**, for 'kite' **DS2T**) presented in OTFT devices excellent performances in air (μ=0.1 cm^2/V s, $I_{on}/I_{off}>10^6$) higher by a factor 5 to the unbridged parent semiconductor (**DS2T**). These results prompted us to associate the rigidification of conjugated system with the introduction of withdrawing groups as carbonyl groups into the bridge in order to increase the electroaffinity and induce a potential n-type character in solid state.

We report here the synthesis and the characterizations of the distyryl end-capped benzo[2,1-*b*:3,4-*b*′]dithiophenes-4,5-dione **1** (Chart 1). As expected structural modifications of **KDS2T** core in **1** lead to a considerable positive shift of the oxidation and reduction potentials in good agreement with spatial representations of the HOMO and LUMO frontier orbitals obtained by density functional theory (DFT). Furthermore, the scanning electron microscopy (SEM) and the crystalline structure characterization by X-ray diffraction (XRD) on **1**-based thin films reveal the drastic change on the morphology with great impact on transport OTFT activity in solid state.

KDS2T

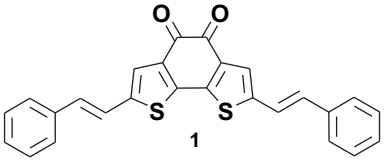

1

Chart 1. Structure of **KDS2T** and diketone **1**.

* Corresponding authors. Tel.: +33 4 94 14 67 24; fax: +33 4 94 14 27 86 (H.B.); tel.: +33 6 17 24 81 93; fax: +33 4 91 82 95 80 (C.V.-A.); e-mail addresses: videlot@cinam.univ-mrs.fr (C. Videlot-Ackermann), brisset@univ-tln.fr (H. Brisset).

0040-4020/$ – see front matter © 2011 Elsevier Ltd. All rights reserved.
doi:10.1016/j.tet.2011.01.006

2. Results and discussion

2.1. Synthesis of the diketone 1

The synthetic route toward **1** is outlined in Scheme 1. The dialdehyde **2** was synthesized as described previously for the synthesis of **KDS2T**.[13] The diketone **1** is obtained by using of potassium cyanide in ethanol.[20] Addition of tetrabutylamonium bromide in the mixture increases the yield of reaction from 3 to 54%.

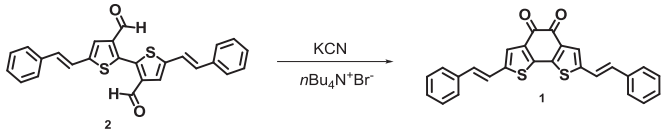

Scheme 1. Synthetic way of diketone **1**.

2.2. UV–vis spectra of diketone 1

As expected for a rigid conjugated system UV–vis spectra of **1** in solution shows a well resolution of the vibronic structure with maxima at 367, 386, and 404 nm together with an absorption band in the low energy range (650 nm) attributed to an intramolecular charge transfer (Fig. 1).[14] UV–vis spectra comparison with unbridged **DS2T** reveals a hypsochromic shift maxima of absorption of 39 nm for diketone **1** indicating a reduction in the effective conjugation length. As for **KDS2T**, this hypsochromic shift can be attributed to the kite shape of bisthienobenzene core, which penalizes the delocalization of the π electrons to form an extended conjugated pathway between both styryl units.[13] Furthermore in the case of **1** the electronic interaction between carbonyl groups and conjugated oligomer backbone can decrease the effective conjugation. A similar observation was reported for copolymers based on cyclopentadithiophenone.[15,16] By extrapolation of the high λ range edge of the absorption spectra a value of 2.60 eV is obtained for the optical bandgap (E_g(opt)), which is 0.23 eV lower compared to **KDS2T**.

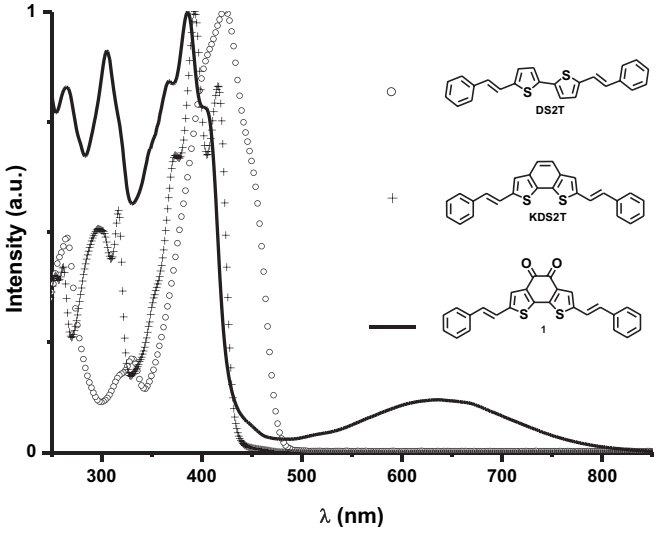

Fig. 1. Absorption spectra of **DS2T**, **KDS2T** and **1** in methylene chloride.

2.3. Cyclic voltammetry of diketone 1

Cyclic voltammogram (CV) of **KDS2T** reveals two reversible one electron redox systems corresponding to the formation of radical cation and radical anion at $E_{1/2}$(ox1)=0.58 V and $E_{1/2}$(red1)=−2.30 V versus Fc/Fc$^+$, respectively.[13] As expected for the diketone **1** compared to **KDS2T** positive shifts are observed for $E_{1/2}$(red1) and $E_{1/2}$(ox1) (−1.00 and 0.82 V versus Fc/Fc$^+$, respectively) due to the electro withdrawing effect of carbonyl groups (Fig. 2). However the effect is more important for $E_{1/2}$(red1) with a positive shift of 1.30 V compared to only 0.24 V for $E_{1/2}$(ox1). Moreover the CV of **1** shows a second redox system in oxidation and reduction corresponding to the formation of dication ($E_{1/2}$(ox2)=1.00 V) and dianion ($E_{1/2}$(red2)=−1.73 V). The reduction wave associated with the first oxidation wave appeared as a sharp cathodic peak characteristic of the adsorption of the oxidized species followed by cathodic desorption from the electrode surface.[17] Contrary as expected, a comparison of the $E_{1/2}$(ox2)–$E_{1/2}$(ox1) and $E_{1/2}$(red2)–$E_{1/2}$(red1) values (0.18 and 0.73 V, respectively) for **1** shows that the dication state is obtained more easily than dianion state after the first redox process indicating that the charges are more separated in the dication state.

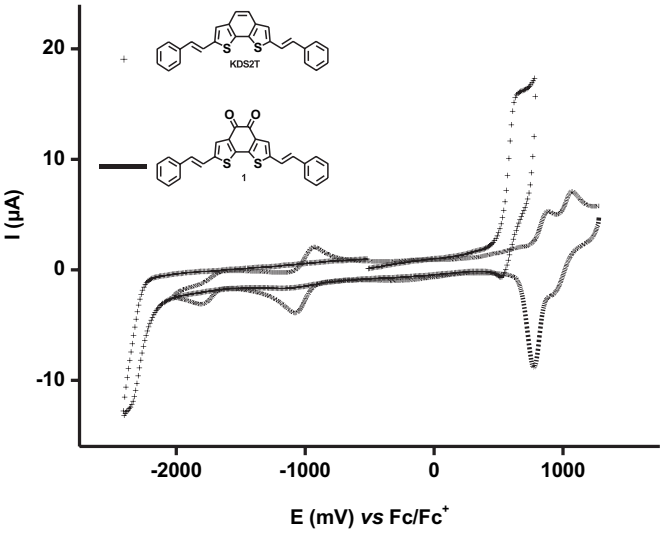

Fig. 2. CV of **KDS2T** (dotted line) and **1** (straight line) at 10^{-3} M in 0,1 M n-Bu_4NPF_6/1,2-dichlorobenzene, v=250 mV.s^{-1}.

2.4. DFT of diketone 1

The spatial representations of the HOMO and LUMO frontier orbitals have been investigated by ab initio quantum calculations with the Gaussian 03 package of programs at a hybrid density functional theory (DFT) level with B3LYP/6-31G(d,p) procedure.[21] HOMO and LUMO levels of neutral molecules **KDS2T** and **1** are shown in Fig. 3. The HOMO of both compounds is located over the

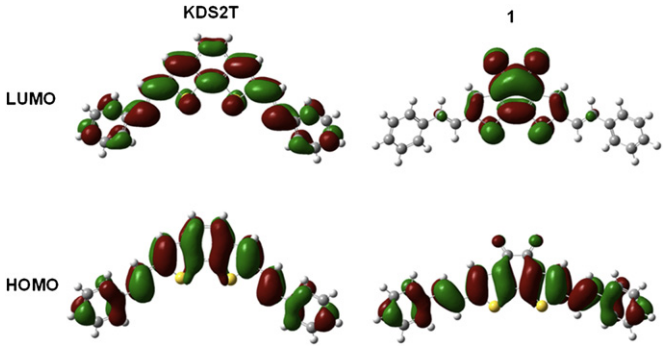

Fig. 3. Spatial representations of HOMO and LUMO levels for **KDS2T** and diketone **1**.

all conjugated system. As contrary distributions of LUMO levels are very different between **KDS2T** and **1**. While LUMO is localized along the entire conjugated system for **KDS2T**, the LUMO level for **1** is mainly localized on the central dithiophene–diketone core. This is in good agreement with electrochemical data and the high value for $E_{1/2}$(red2)−$E_{1/2}$(red1) indicating that negative charges are locating on the dithiophene core.

E_{HOMO} is estimated from $E_{1/2}$(ox1) and E_{LUMO} from the relation $E_{LUMO}=E_{HOMO}+E_g$(opt).[18,19] HOMO/LUMO energies levels are estimated as follows for **KDS2T** (−5.42/−2.94) and diketone **1** (−5.66/−3.06) versus **DS2T** (−5.32/−2.72 eV) and reported on an energy diagram (Fig. 4). The electrochemically derived LUMO energies decrease continuously from **DS2T**, **KDS2T** to **1**, which is consistent with an increase of electroaffinity due to the rigidification and introduction of electron-withdrawing groups on the conjugated core.

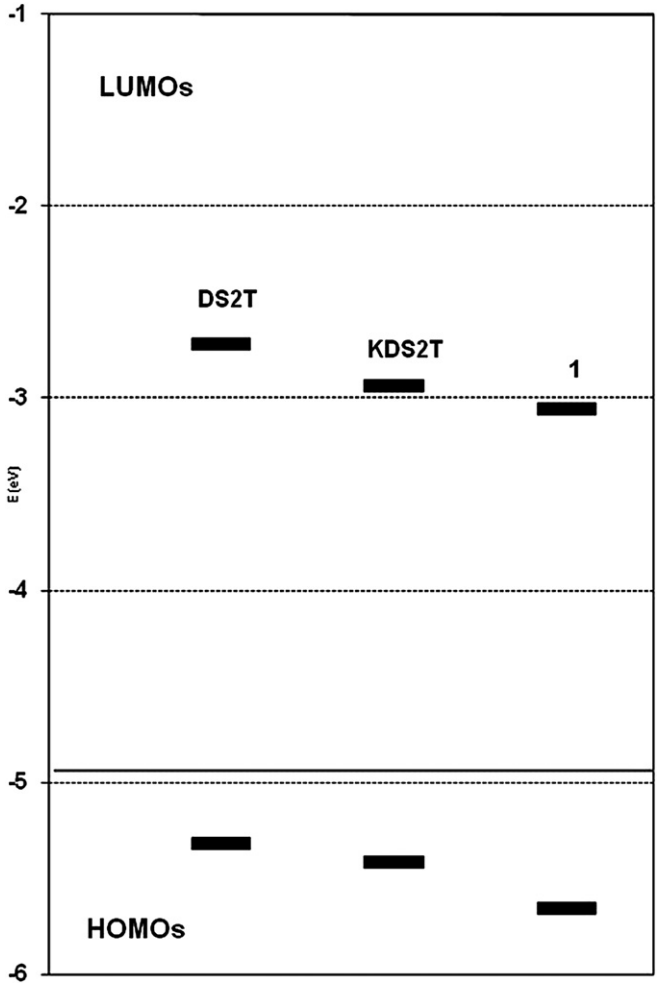

Fig. 4. Energy diagram of LUMO and HOMO energies for **DS2T**, **KDS2T** and **1** based on experimental and DFT. The horizontal thick line corresponds to Fermi level of gold electrode (4.9 eV).

2.5. Thin films characteristics

$\theta/2\theta$ X-ray diffraction spectra of **1**-based thin films vacuum-deposited at 80 °C, with a nominal thickness of 50 nm reveal that the films are characterized by sharp and small reflections (Fig. 5). The peaks can be indexed from the (001) to (004) reflection, indicating that the *ab*-planes of the grains are oriented parallel to the substrate surface. To compare to the peaks indexed up to 14th order in highly oriented polycrystalline **KDS2T** based film,[13] the low occurrence of (00*l*) progressions until only four reflections suggests a low microstructural order of **1**-based thin films. However, the interplanar *d*(001)-spacing of 1.97 nm is similar to the value found for **KDS2T** based film (1.98 nm), which corresponds to the molecular length of **KDS2T** determined by the single-crystal X-ray analysis.[13] This result suggests that the shape of **1** is identical to **KDS2T** and molecules are nearly perpendicular onto the substrate with a molecular tilt angle of ∼18° to the normal of the substrate.

Characterization of the thin film microstructure at the interface with the substrate, the active region for charge transport in OTFTs, is challenging by conventional techniques, therefore it is often evaluated by scanning electronic microscopy (SEM). Fig. 6 shows the surface morphology of **1**-based thin films as 50 nm thick vacuum-deposited layers on Si/SiO_2 substrates heated at 80 °C. Numerous grains appear with identical sizes, height and shape homogeneously deposited on the surface together with no well defined grain boundary. The order observed by XRD is located in the bulk of such grains as no terraces are observed on top of grains.

Top-contact thin-film transistors were fabricated in the manner described in the Experimental part. Drain and source Au electrodes were deposited on top of the semiconducting layer after the latter was evaporated onto untreated and HMDS-treated Si/SiO_2 substrates at temperature (T_{sub}) of either 30 °C or 80 °C. All measurements were performed in air at room temperature. Any field-effect activity either under positive or negative voltages is measured probably due to the low microstructural order of thin films.

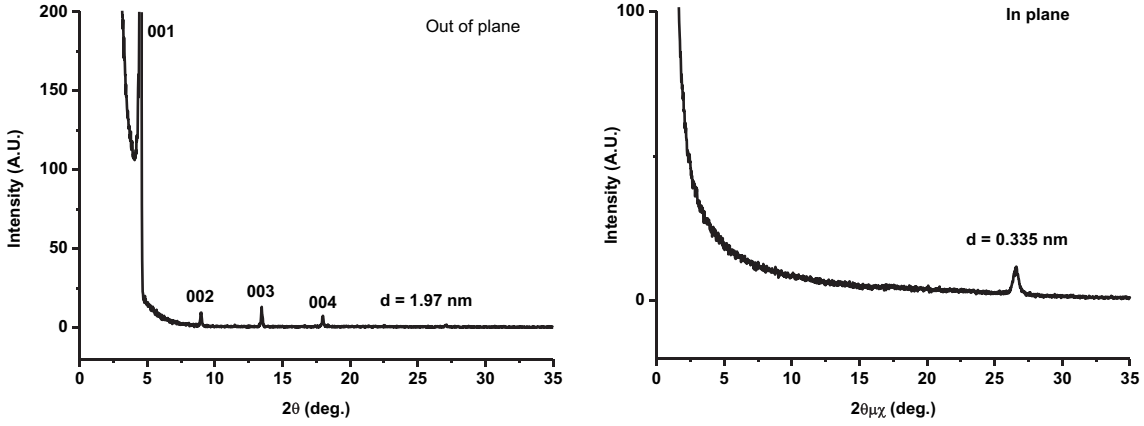

Fig. 5. $\theta/2\theta$ Mode of X-ray diffraction patterns of **1**-thin film deposited at T_{sub}=80 °C on Si/SiO_2 with a nominal thickness of 50 nm.

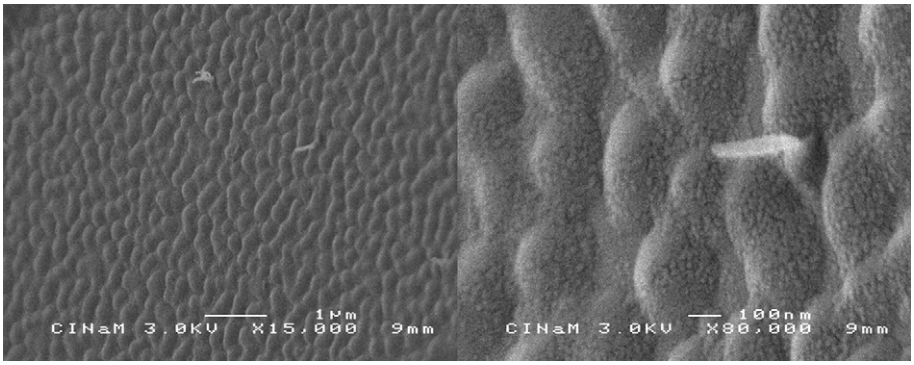

Fig. 6. SEM pictures of diketone **1** thin films as 50 nm thick vacuum-deposited layers on Si/SiO_2 substrates heated at 80 °C.

3. Conclusion

In conclusion, a novel bridged distyryldithiophene with ketone groups on the bridge was prepared. As expected an important positive shift of reduction potential was observed indicating an increase of the electroaffinity. Unfortunately **1**-based films reveal a low microstructural order in solid state preventing any efficient charge transport in air.

4. Experimental

4.1. Synthesis

Ethanol, methylene chloride, toluene were purchased from CarloErba. Tetrabutylamonium bromide and hexafluorophosphate (TBHP) were purchased from Fluka and silica gel (240–400 mesh) from Merck. 1,2-Dichlorobenzene was purchased from Sigma–Aldrich. Compound **2** was prepared as described previously.[13] Melting point is uncorrected and was obtained from an Electrothermal 9100 apparatus. ^1H NMR and ^{13}C NMR spectra were recorded on Bruker AC 250 at, respectively, 250 MHz and 62.5 MHz.

*4.1.1. E,E-2,7′-Bis((2-phenyl)-ethenyl)-benzo[2,1-b:3,4-b′]dithiophene-4,5-dione **1**.* To a refluxing mixture of 0.10 g (0.24 mmol) of **2** in 10 mL of ethanol is added 0.04 g (0.60 mmol) of potassium cyanide[20] in 5 mL of water tetrabutylammonium bromide (3%). After 12 h of stirring under reflux, the mixture is cooled before adding methylene chloride. After extraction, drying, filtering and solvent evaporation under vacuum, the crude product is purified by chromatography under silica gel with toluene to give 0.06 g (54%) of blue solid corresponding to the title compound. Mp=253–254 °C. ^1H NMR (250 MHz, $CDCl_3$) δ: 6.91 (d, ^3J=15.95 Hz, 2H, H_{eth}), 7.10 (d, ^3J=16.12 Hz, 2H, H_{eth}), 7.34 (s, 2H, H_{thio}), 7.30–7.47 (m, 10H, H_{phe}). ^{13}C NMR (67.5 MHz, $CDCl_3$) δ: 119.88, 125.30, 126.69, 128.68, 128.89, 131.50, 135.71, 141.75, 143.45, 174.17, 181.64 (C=O). UV (CH_2Cl_2) (log ε): 228 (4.73), 265 (4.67), 367 (4.96), 367 (4.97), 386 (5.05), 404 (4.94), 635 (4.13). SM (ESI^+) m/z: 425 $[M+H]^+$, 442 $[M+NH_4]^+$, 447 $[M+N]^+$.

4.2. Solution measurements

Cyclic voltammetric (CV) data were acquired using a BAS 100 Potentiostat (Bioanalytical Systems) and a PC computer containing BAS 100W software (v2.3). A three-electrode system with a Pt working electrode (diameter 1.6 mm), a platinum counter electrode, and an Ag/AgCl (with 3 M NaCl filling solution) reference electrode was used. Tetrabutylammonium hexafluorophosphate (TBHP) (Fluka) was used as received. Anhydrous 1,2-dichlorobenzene has an electronic grade purity. Each compound was at 1×10^{-3} M in 1,2-dichlorobenzene/TBHP 0.1 M. $E_{1/2}$ redox values are determined from the cyclic voltammogram at a scan rate of 50 mV s^{-1}. Ferrocene was used as internal standard. UV–vis absorption spectra were obtained on a Varian Cary 1E spectrophotometer.

4.3. Theoretical details

Spatial representations of the HOMO and LUMO frontier orbitals have been investigated by ab initio quantum calculations with the Gaussian 03 package of programs at a hybrid density functional theory (DFT) level with B3LYP/6-31G(d,p) procedure.[21]

4.4. Film characterizations

Scanning electronic microscopy (SEM) pictures were realized by a JEOL field emission gun scanning electron microscope (FEG-SEM, model JSM 6320F). Thin films of **1**, analyzed by X-ray film diffractometry (XRD), were fabricated by vacuum deposition in a pressure of 5×10^{-5} Pa using K-cell type crucible. Si wafer (covered by SiO_2 layer 300 nm thick) was used as substrates. The substrate temperature (T_{sub}) was controlled to be 80 °C by heating the block on which the substrates are mounted. The deposition rate was 6 nm/min. The final film thickness was 50 nm. The as-deposited thin films were characterized using X-ray diffraction in air using an X-ray diffractometer (Regaku Co., ATX-G), which was specially designed for characterization of thin films. Both in-plane and out-of-plane diffractions could be measured, because the goniometer has not only conventional $\theta/2\theta$ axes but also in-plane $\theta/2\theta\chi$ axes. The used wavelength of X-ray in the experiments was 0.1542 nm.

4.5. OTFTs fabrication

The top contact configuration was used for the OTFT devices based on **1**. Highly n-doped silicon wafers (gate), covered with thermally grown silicon oxide SiO_2 (300 nm, insulating layer), were purchased from Vegatec (France) and used as device substrates. Hexamethyldisilazane (HMDS) treatment was carried out by immersing the Si/SiO_2 substrate in a pure HMDS solution at room temperature overnight. The capacitance per unit area of either untreated or HMDS-treated silicon dioxide dielectric layers was $1.2–1.3\times10^{-8}$ F/cm^2. The semiconductor layer was vacuum-deposited onto the insulating layers, using an Edwards Auto 306 apparatus, at a rate of 4–7 nm/min under a pressure of $1–2\times10^{-6}$ mbar to a nominal thickness of 50 nm as determined with a in situ quartz crystal monitor. Substrate temperature (T_{sub}) during deposition was controlled by heating or not, the block on which the substrates are mounted. The substrate temperature was fixed to 30 °C or 80 °C. The Au source and drain electrodes (channel length L=50 μm, channel width W=1 mm) were evaporated on top of the organic thin film through a shadow mask. Hewlett-Packard 4140B pico-amperemeter–DC voltage source is used to apply an increasing drain-source voltage (V_D) under a constant gate voltage

(V_G). Positive or negative voltages can be ranged from 0 to |100| V. All measurements were performed in air.

Acknowledgements

The authors acknowledge S. Nitsche and D. Chaudanson from CINaM for SEM pictures. Pr F. Fages is gratefully acknowledged for his fruitful discussions.

References and notes

1. Murphy, A. R.; Fréchet, J. M. J. *Chem. Rev.* **2007**, *107*, 1066–1096.
2. Facchetti, A. *Mater. Today* **2007**, *10*, 28–37.
3. Mishra, A.; Ma, C.-Q.; Bäuerle, P. *Chem. Rev.* **2009**, *109*, 1141–1276.
4. Videlot-Ackermann, C.; Ackermann, J.; Brisset, H.; Kawamura, K.; Yoshimoto, N.; Raynal, P.; El Kassmi, A.; Fages, F. *J. Am. Chem. Soc.* **2005**, *127*, 16346–16347.
5. Videlot-Ackermann, C.; Ackermann, J.; Kawamura, K.; Yoshimoto, N.; Brisset, H.; Raynal, P.; El Kassmi, A.; Fages, F. *Org. Electron.* **2006**, *7*, 465–473.
6. Mauldin, C. E.; Puntambekar, K.; Murphy, A. R.; Liao, F.; Subramanian, V.; Fréchet, J. M. J.; DeLongchamp, D. M.; Fischer, D. A.; Toney, M. F. *Chem. Mater* **2009**, *21*, 1927–1938.
7. Liu, P.; Wu, Y.; Pan, H.; Li, Y.; Gardner, S.; Ong, B. S.; Zhu, S. *Chem. Mater.* **2009**, *21*, 2727–2732.
8. Videlot-Ackermann, C.; Brisset, H.; Zhang, J.; Ackermann, J.; Nénon, S.; Fages, F.; Marsal, P.; Tanisawa, T.; Yoshimoto, N. *J. Phys. Chem. C* **2009**, *113*, 1567–1574.
9. Didane, Y.; Marsal, P.; Fages, F.; Kumagai, A.; Yoshimoto, N.; Brisset, H.; Videlot-Ackermann, C. *Thin Solid Films* **2010**, *519*, 578–586.
10. Didane, Y.; Martini, C.; Barret, M.; Sanaur, S.; Collot, P.; Ackermann, J.; Fages, F.; Brisset, H.; Videlot-Ackermann, C. *Thin Solid Films* **2010**, *518*, 5311–5320.
11. Didane, Y.; Diallo, A. K.; Fiorido, T.; Suzuki, A.; Yoshimoto, N.; Bernardini, S.; Ackermann, J.; Fages, F.; Brisset, H.; Bendahan, M.; Aguir, K.; Videlot-Ackermann, C. *J. Optoelectron. Adv. Mater.* **2010**, *12*, 1546–1551.
12. Fiorido, T.; Bendahan, M.; Aguir, K.; Bernardini, S.; Martini, C.; Brisset, H.; Fages, F.; Videlot-Ackermann, C.; Ackermann, J. *Sens. Actuators B: Chem.* **2010**, *151*, 77–82.
13. Didane, Y.; Mehl, G. H.; Kumagai, A.; Yoshimoto, N.; Videlot-Ackermann, C.; Brisset, H. *J. Am. Chem. Soc.* **2008**, *130*, 17681–17683.
14. Rieger, R.; Enkelmann, V.; Müllen, K. *Materials* **2010**, *3*, 1904–1912.
15. Li, K.-C.; Hsu, Y.-C.; Lin, J.-T.; Yang, C.-C.; Wei, K.-H.; Lin, H.-C. *J. Polym. Sci., Part A: Polym. Chem.* **2009**, *47*, 2073–2092.
16. Yen, W.-C.; Pal, B.; Yang, J.-S.; Hung, Y.-C.; Lin, S.-T.; Chao, C.-Y.; Su, W.-F. *J. Polym. Sci., Part A: Polym. Chem.* **2009**, *47*, 5044–5056.
17. Bard, A. J.; Faulkner, L. R. *Electrochemical Methods*, 2nd ed.; Wiley: New York, NY, 2001.
18. Yoon, M.-H.; DiBenedetto, S. A.; Facchetti, A.; Marks, T. J. *J. Am. Chem. Soc.* **2005**, *127*, 1348–1349.
19. Facchetti, A.; Mushrush, M.; Katz, H. E.; Marks, T. J. *Adv. Mater.* **2003**, *15*, 33–38.
20. Wynberg, H.; Sinnige, H. J. M. *Recl. Trav. Chim. Pays-Bas* **1969**, *88*, 1244–1245.
21. Frisch, M. J.; Trucks, G. W.; Schlegel, H. B.; Scuseria, G. E.; Robb, M. A.; Cheeseman, J. R.; Montgomery, J. A., Jr.; Vreven, T.; Kudin, K. N.; Burant, J. C.; Millam, J. M.; Iyengar, S. S.; Tomasi, J.; Barone, V.; Mennucci, B.; Cossi, M.; Scalmani, G.; Rega, N.; Petersson, G. A.; Nakatsuji, H.; Hada, M.; Ehara, M.; Toyota, K.; Fukuda, R.; Hasegawa, J.; Ishida, M.; Nakajima, T.; Honda, Y.; Kitao, O.; Nakai, H.; Klene, M.; Li, X.; Knox, J. E.; Hratchian, H. P.; Cross, J. B.; Adamo, C.; Jaramillo, J.; Gomperts, R.; Stratmann, R. E.; Yazyev, O.; Austin, A. J.; Cammi, R.; Pomelli, C.; Ochterski, J. W.; Ayala, P. Y.; Morokuma, K.; Voth, G. A.; Salvador, P.; Dannenberg, J. J.; Zakrzewski, V. G.; Dapprich, S.; Daniels, A. D.; Strain, M. C.; Farkas, O.; Malick, D. K.; Rabuck, A. D.; Raghavachari, K.; Foresman, J. B.; Ortiz, J. V.; Cui, Q.; Baboul, A. G.; Clifford, S.; Cioslowski, J.; Stefanov, B. B.; Liu, G.; Liashenko, A.; Piskorz, P.; Komaromi, I.; Martin, R. L.; Fox, D. J.; Keith, T.; Al-Laham, M. A.; Peng, C. Y.; Nanayakkara, A.; Challacombe, M.; Gill, P. M. W.; Johnson, B.; Chen, W.; Wong, M. W.; Gonzalez, C.; Pople, J. A; Gaussian 03, Revision B.04. Gaussian: Wallingford, CT, 2004.